ADVANCES IN MATERIALS SCIENCE, Vol. 24, No. 3 (81), September 2024

DOI: 10.2478/adms-2024-0014

Karolina Płatek[1], Leszek Łatka[1, *], Monika Nowakowska[1]

[1]Department of Metal Forming, Welding and Metrology, Faculty of Mechanical Engineering, Wroclaw University of Science and Technology, Wroclaw, Poland

***** *leszek.latka@pwr.edu.pl*

THE INFLUENCE OF INJECTION MODE AND SPRAY DISTANCE ON WEAR RESISTANCE OF Al_2O_3+13 WT.% TiO_2 COATINGS

ABSTRACT

Atmospheric plasma spraying (APS) allows deposition of ceramic coatings on metallic substrate, significantly increasing the wear resistance of the component. Coating's microstructure and consequently its properties, depend on heat treatment of the feedstock particles. This property can be controlled by process parameters, especially electric power and spray distance. On the other hand, some plasma torches allow introducing another variable, an injection mode, which could be realized in external or in internal way. In the presented research, wear resistance of Al_2O_3+13 wt.% TiO_2 coatings deposited under various values of spray distance and different injection modes were examined using ASTM G-99 procedure. The impact of spraying parameters on the coating's microstructure was established and connected to the functional properties of the manufactured deposits. Observed differences indicated influence of injection mode and spray distance value. Coatings deposited with internal feedstock injection exhibit lower porosity and slightly higher hardness than these made with external injection mode. In terms of wear resistance for both spray distance the wear factor was lower for internal injection system. Obtained results confirmed assumed thesis, that internal injection mode improves heat treatment and consequently ameliorate wear performance of plasma sprayed alumina-titania coatings.

Keywords: *atmospheric plasma spraying; wear resistant coatings; injection system; spraying distance*

INTRODUCTION

Improving the abrasive wear resistance of a material's surface is crucial for enhancing the lifespan of components. Ceramic materials are renowned for their excellent resistance to abrasion and erosion [1,2]. However, the challenges in the manufacturing of ceramics significantly limit their potential applications. To overcome this issue, ceramics are often implemented in the form of a coating. For deposition of such coating, various methods are used, with atmospheric plasma spraying (APS) being one of the most promising [3]. APS, thanks to its ability to generate high temperatures reaching up to 20,000 K, enables the relatively efficient, one-step deposition of

Received: 2024.06.01; Received in revised form: 2024.06.28; Accepted: 2024.06.28

ceramic coatings onto metallic substrates [4]. The feedstock material used for coating deposition typically has a form of powder. Upon deployment into the plasma stream, the feedstock material is heated and accelerated to high velocities (starting from 100 m/s, up to 300 m/s) toward the substrate. Upon impact, the partially melted particles deform to form a flattened 'splat,' contributing to the successive growth of the coating. The successive growth of these splats results in the development of the coating [5,6].

Among materials commonly used in the APS process, Al_2O_3 and TiO_2 are especially popular. Due to their high hardness, good adhesion, and excellent abrasive wear resistance, Al_2O_3 coatings are already widely used for components in turbines, bearings, and biomedical implants. The anti-wear properties of this material have been widely described in paper [7]. Although the low fracture toughness of Al_2O_3 is limiting its range of applications. This property can be improved by the addition of TiO_2 [8,9]. The addition of TiO_2 is especially profitable in the case of coatings manufactured using thermal spray methods. According to the Al_2O_3-TiO_2 phase diagram, around 13 wt.% of TiO_2, the melting temperature of the mixture is reduced. Consequently, an increase in compactness, bonding strength, and toughness of the plasma sprayed coatings is observed, as well as decrease in porosity level [10,11]. Moreover, the efficiency of spraying process is higher. Thanks to superior anti-wear properties and relatively low cost, Al_2O_3-TiO_2 coatings are widely used in various branches including, inter alia, biomedical, marine and aeronautics [12–14].

The quality of plasma sprayed coating depends on the morphology and properties of the feedstock material, as well as on spraying conditions. Among various plasma spraying parameters, plasma torch power, spraying distance, and the flow rate of plasma-forming gas are considered the most decisive factors [15,16]. The heating of the particles is highly influenced by the spraying distance, which refers to the distance between the nozzle and the surface of the substrate material. The spraying distance determines the times spent by the particles in the plasma jet: when it is too short, the particles cannot reach the proper temperature allowing formation of splats. On the other hand, when the distance is too long, the cooling of the particles may occur. Thus, proper adjustment of this parameter is crucial for coating properties [17,18].

Although besides spraying parameters, the properties of coatings can also be affected by the type of feedstock injection system. Two main types of injection systems can be distinguished: internal and external systems. In the internal injection system, the powder is introduced directly into the plasma jet inside the nozzle of the plasma torch. This solution provides precise location of injection and provides that the feedstock material will be evenly heated, despite the differences in particle size. On the other hand, using external injection with the injector mounted at a short distance from the nozzle facilitates control of injection parameters and reduces perturbation in the plasma jet flow [19]. Usually, the external injection system is applied, and only a few studies comparing both injections systems were found [20,21], whereas our previous study showed high influence of injection system on coatings properties, indicating the need for further examination [22].

In the presented research, the APS process was applied for deposition of Al_2O_3-13wt.%TiO_2 coatings using external and internal systems along with different spraying distances. As a result, the impact of injection type and spraying distance on morphology, hardness, and wear resistance of Al_2O_3-13wt.%TiO_2 plasma sprayed coatings was examined. The wear resistance was tested using ball-on-disc tribometer in dry friction conditions, with the guidelines prescribed in ASTM G-99 standard [23].

MATERIALS AND METHODS

Commercially available Al_2O_3 + 13 wt.% TiO_2 powder (Metco 6221) provided by Oerlikon (Oerlikon Metco AG, Wohlen, Switzerland) was used as the feedstock. The feedstock material was examined for size, morphology, and phase composition. The size distribution was determined by laser diffraction using PSA 1190 particle size analyzer (AntonPaar, Graz, Austria). The results showed that the volume–surface mean diameter d_{v50} of the powder particles was 33.3 µm. SEM observations using JEOL JSM-6610A (Jeol, Tokyo, Japan) revealed that the particles exhibit a morphology typical for agglomerated and sintered powders, with spheroidal shape consisting of numerous fine particles. XRD analysis revealed the presence of α-Al_2O_3, rutile-TiO_2, and tialite Al_2TiO_5 phases. The examination procedure, as well as its results, have already been described in detail in the article [24].

The SG-100 (Praxair, Indianapolis, In, USA), one-cathode – one anode, plasma torch was used for coating deposition on the 1.4301 austenitic stainless steel discs. The plasma torch was attached to a 6-axis Fanuc 2000 IA robot, while the substrates were mounted on the rotating carousel, as presented in Fig. 1. The diameter of the discs was 25 mm, and the thickness was 2 mm. Prior to spraying, substrate material was sand blasted using F40 corundum grit and cleaned with ethanol. On top of the substrate, Ni20Cr bondcoat with the thickness of 150 µm was deposited using APS method.

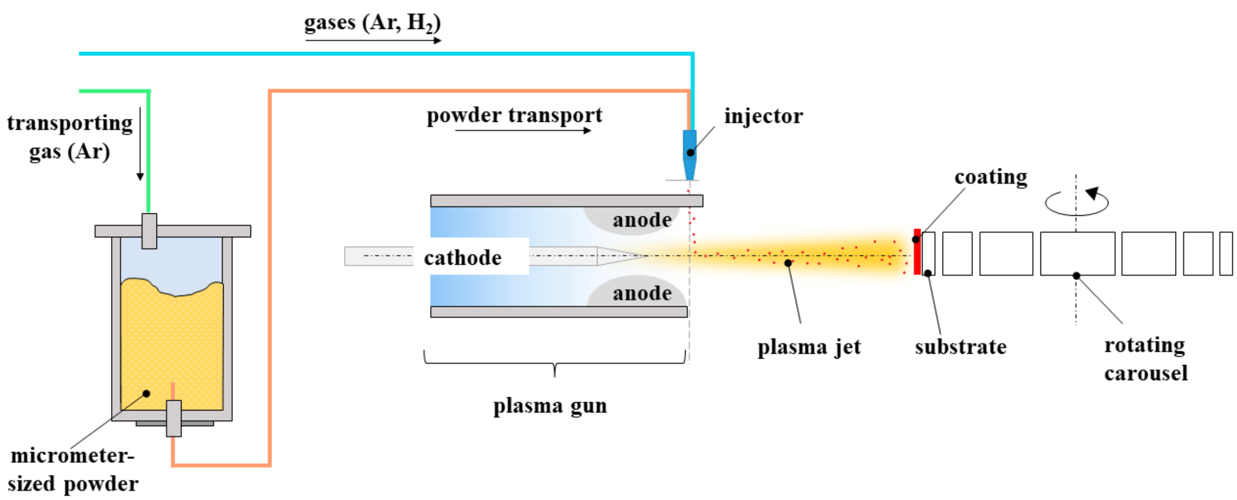

Fig. 1. The schematic representation of the spraying process based on [24]

For plasma generating, a mixture of Ar and H_2 was used with a gas flow rate of 45 slpm and 5 slpm respectively. The power of the plasma torch was established at the constant level of 39 kW. As feedstock carrier gas, Ar with a stable flow rate of 3 slpm was used. To avoid clogging during powder feeding, the feedstock materials were dried for 2 hours at the temperature of 120 °C.

The examined variables were: (i) spraying distance and (ii) injection type. In the case of the external injection, the powder was introduced into plasma jet at the distance of 4 mm from the axis of the nozzle. In both cases, the injector was positioned perpendicularly to the axis of the nozzle. The schematic representation of the examined injection systems is presented in Fig. 2.

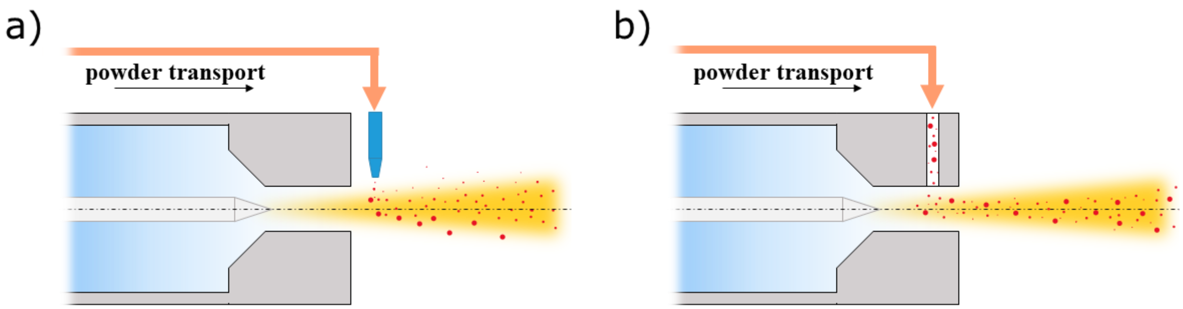

Fig. 2. Schematic representation of feedstock injection systems: a) external, b) internal

Two values of spraying distance, 80 and 100 mm, were examined for both types of injection systems. The process variables and corresponding sample codes are listed in Table 1.

Table 1. *Process variables and sample codes*

Sample code	Injection type	Spraying distance, mm
E80	External	80
E100	External	100
I80	Internal	80
I100	Internal	100

The microstructure of deposited coatings was observed at the top surface and cross-section using scanning electron microscope Tescan Vega 3 (Tescan, Brno, Czech Republic) and Keyence VHX 6000 digital microscope (Keyence, Mechelen, Belgium). Cross-section images obtained from the digital microscope were used to measure the coating thickness, while SEM images were used for morphology examination and porosity measurement. Porosity was calculated following ASTM E2109-01 standard using automated analysis algorithm (method B) [25]. For each sample, 25 images were taken under x1000 magnification using BSE mode, and the average porosity value was calculated.

The hardness of the coatings was measured using the Vickers method with an HV-100 hardness tester provided by Sinowon Innovation Metrology (Dongguan, China). For each sample, 10 imprints were taken in the random places of the coatings cross-sections, under the load of 1.96 N (HV0.2). The procedure followed the ISO 4516 standard [26].

The sliding wear test was carried out in accordance with ASTM G-99 dry sliding wear test procedure [23] using MFT-5000 apparatus (Rtec Instruments, San Jose, CA, USA). Coatings were tested against a 6 mm diameter ball made from WC with the addition of 6 wt.% of Co. The counterbody was pressed against the tested surfaces with a stable load of 20 N. Given the linear velocity of 0.1 m/s and wear track radius of 8 mm, the total sliding distance of 250 m was reached in 42 min. Before testing, the coatings were ground and polished to achieve surface roughness Ra < 1 μm. During the test, the coefficient of friction (CoF) was recorded. The wear factor K of the coatings was calculated based on the volume loss ΔV, mm^3, obtained from Keyence VHX 6000 digital microscope using following formula (1):

$$K = \frac{\Delta V}{F \cdot S} \quad (1)$$

where *F* denotes to the press force in N, and *S* means the total sliding distance in *m* [27]. After testing, the morphology of the wear tracks was examined using SEM.

RESULTS AND DISCUSSION

The microstructure of the coatings surface is shown in Fig. 3.

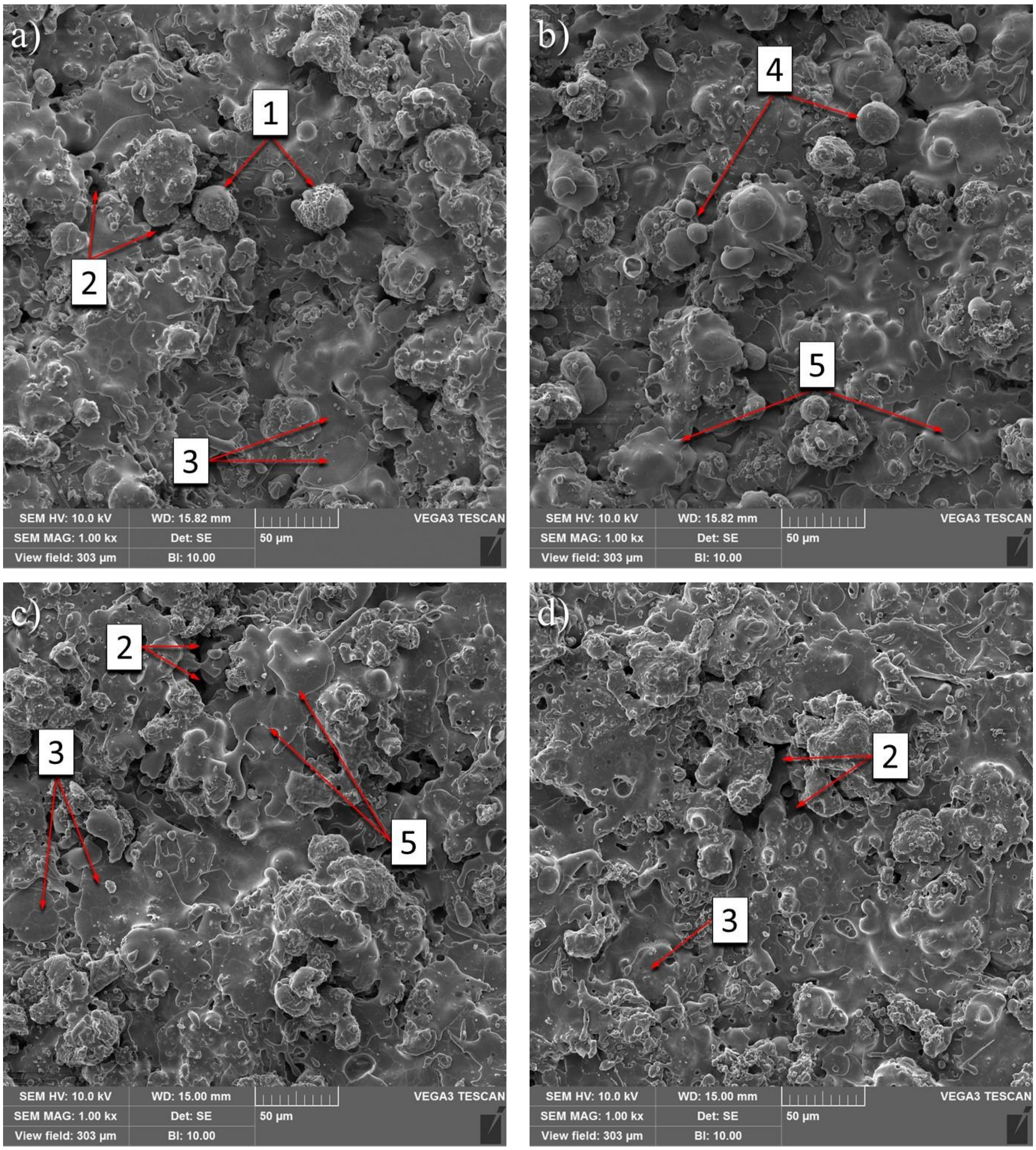

Fig. 3. SEM micrographs of the coatings: a) E80, b) E100, c) I80, d) I100; with marked structures: 1 – partially melted particles, 2 – open porosity, 3 – cracks, 4 – remelted particles, 5 – splats

The morphology of the deposited coatings is typical for this spraying method and in all cases consist of splats and partially melted particles, with some pores, voids, cracks and remelted particles [28,29]. Although the amount of each structure varies between the samples. The number of unmelted particles, along with accompanying pores and voids, is highest in the case of E80 (Fig. 3a). On the other hand, the increase in spraying distance resulted in cooling down of the in-flight particles, reducing their tendency to undergo plastic deformation during impact. Such remelted partciles can be spotted on the surface of the E100 sample (Fig. 3b). The consequences of this phenomenon include a higher porosity percentage and a dual structure consisting of melted and partially melted regions [30]. However, coatings sprayed from the shorter distance exhibit more cracks due to high heat input, what is visible in Fig. 3c and Fig. 3d. Additionally, the shorter spraying distance resulted in predominance of disc-shaped splats over fragmented ones, what is connected to the greater substrate heating [31]. The coatings deposited using internal injection exhibit a more complex structure, resulting from higher diversity in particle size.

In Fig. 4, the cross-section of the samples E100 (Fig. 4a and 4b) and I80 (Fig. 4c and Fig. 4d). The observations were performed using both digitl and SEM microscope.

The thickness of deposited coatings varies significantly between samples produced by internal and external injection. In the first case, the thickness did not exceed 446 ± 27 μm, while with internal powder injection, it reached 650 ± 20 μm. With external powder injection, particles with diameters that are either too small or too large are reflected or passed through the plasma jet, respectively, due to improper angular momentum. As a result, only a specific fraction of the particles reaches the substrate, leading to a dramatic decrease in the efficiency of the plasma spraying process [32]. Internal injection reduces this phenomenon to some extent and allows for higher deposition rates [20,21].

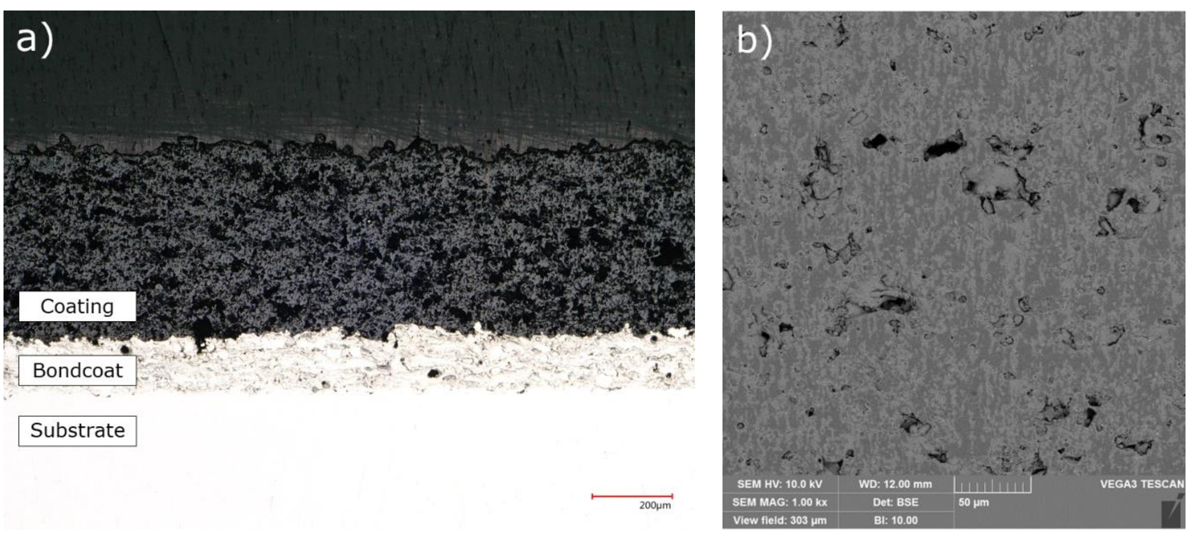

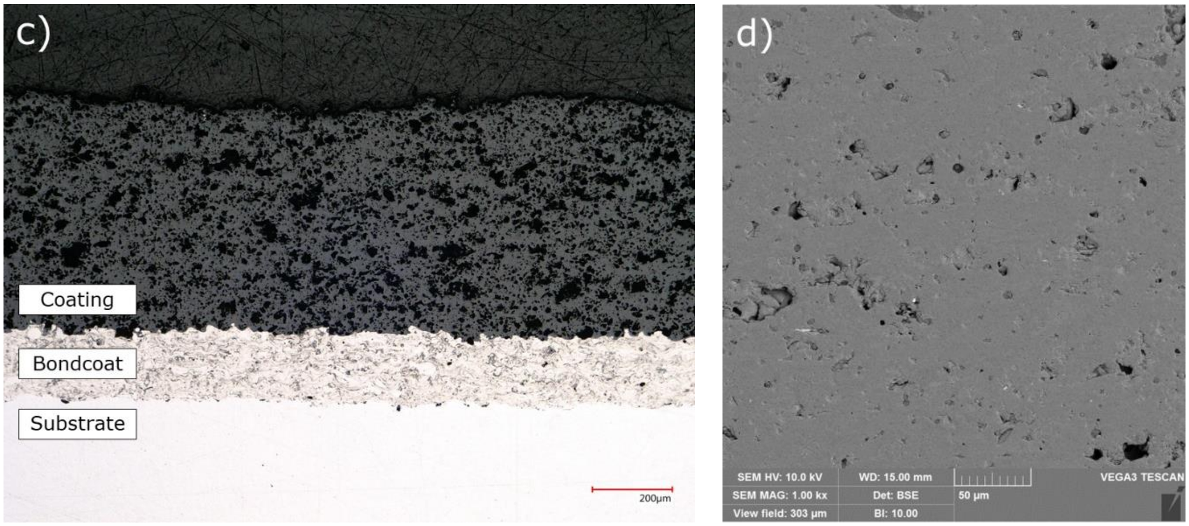

Fig. 4. Cross-section of the coatings a), b) E100 and c), d) I80, observed using a), c) digital and b), d) SEM microscope

The differences in coating thickness between samples deposited using the same type of injection system may partially result from differences in the porosity value. In both cases, the samples deposited at higher distance present higher thickness and higher porosity level. Although the overall porosity percentage of the coatings ranged from 4.1 ± 0.7 to 5.3 ± 0.9%. The porosity level stands in line with the literature [33]. The obtained results are slightly better than those presented in our previous study [22]. This divergence is most likely related to the difference in the torch power, which, in case of the previous study, had a value of 35 kW.

The hardness of the coatings ranges from 909 ± 141 to 966 ± 128 HV0.2. The results are similar to that obtained by other researchers [34,35]. The standard deviation of hardness is lower for samples with lower porosity levels, as their structure is more homogeneous. Detailed information about the thickness, porosity, and hardness of the coatings is listed in Table 2.

Table 2. *Properties of the deposited coatings*

Sample	Thickness, µm	Porosity, %	Hardness, HV0.2
E80	412 ± 22	5.1 ± 1.3	909 ± 141
E100	446 ± 27	5.3 ± 0.9	940 ± 178
I80	579 ± 21	4.1 ± 0.7	966 ± 128
I100	650 ± 20	4.4 ± 1.0	952 ± 181

The results of the sliding wear test are presented in Fig. 5. The I80 sample exhibits the best sliding wear resistance among the tested coatings, with a value of 18.55 ± 7.8 $mm^3\ N^{-1}\ m^{-1} \cdot 10^{-6}$. This outcome can be correlated with the type of injection system and its impact on powder heating. With internal injection, the feedstock's exposure to the heat generated by the plasma torch is extended compared to external injection, resulting in higher particle plasticity. Additionally, the particles are evenly heated, despite differences in particle sizes. This leads to easier formation of the splats and stronger cohesion between them. The wear resistance of the coatings correlates with the hardness of the coating, what stands in line with the literature [36,37]. On the other hand, the cohesion between splats deposited from higher distances may be weakened due to insufficient particle melting, what is also reflected by higher porosity level. The influence of pore distribution on mechanical properties of plasma sprayed coatings has been widely described in paper [33].

On the other hand, the lowest wear resistance was measured for E100 sample (29.16 ± 5.3 $mm^3 N^{-1} m^{-1} \cdot 10^{-6}$). In all cases, the coefficient of friction ranged from 0.20 to 0.25 within testing.

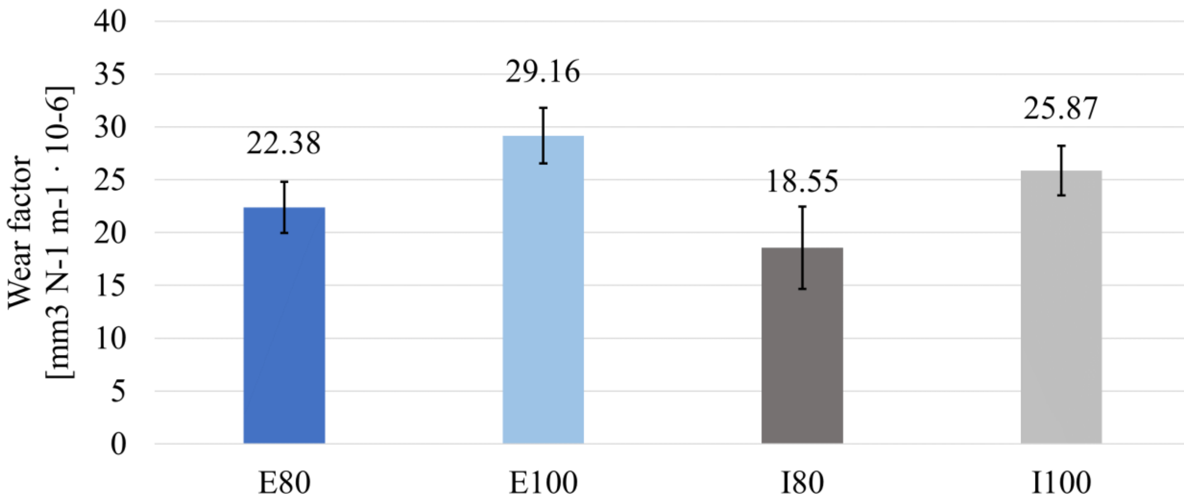

Fig. 5. The results of dry sliding wear test

After testing, the resulting wear tracks were observed using SEM microscope (Fig. 6). The observations revealed that a few mechanisms contributed to the wear of the coatings: low-cycle fatigue, delamination and abrasive wear related to the three-body abrasion phenomenon [38]. The surface of the wear tracks is marked by the cracks, perpendicular to the sliding direction, what is typical for fatigue wear mechanism [39]. These cracks results from drag-tearing of the material by the counter body, typical for this mechanism of wear. As a results, the splats undergo delamination. An example of this phenomenon is presented in Fig. 6a and Fig. 6b. On the other hand, when material cracks, some loose debris is transferred to the space between the counterbody and tested surface. This debris is furthermore moved by the movement between the coating and counterbody causing the three-body abrasive wear [40]. The results of this mechanism are visible in Fig. 6b as short, curvilinear scratches and micro-ploughs. The finding stands in line with the literature [41].

The correlation between the porosity level and sliding wear resistance may partially results from the phenomenon presented in Fig. 6c and Fig. 6d. The closer look at the crack shows that under the load of the counterbody, the material collapsed into to the void located near the coatings surface. As a result, a large pit was created. Besides this, the pores may also act as a starting point for the crack and splats delamination, what is also visible in Fig. 6d.

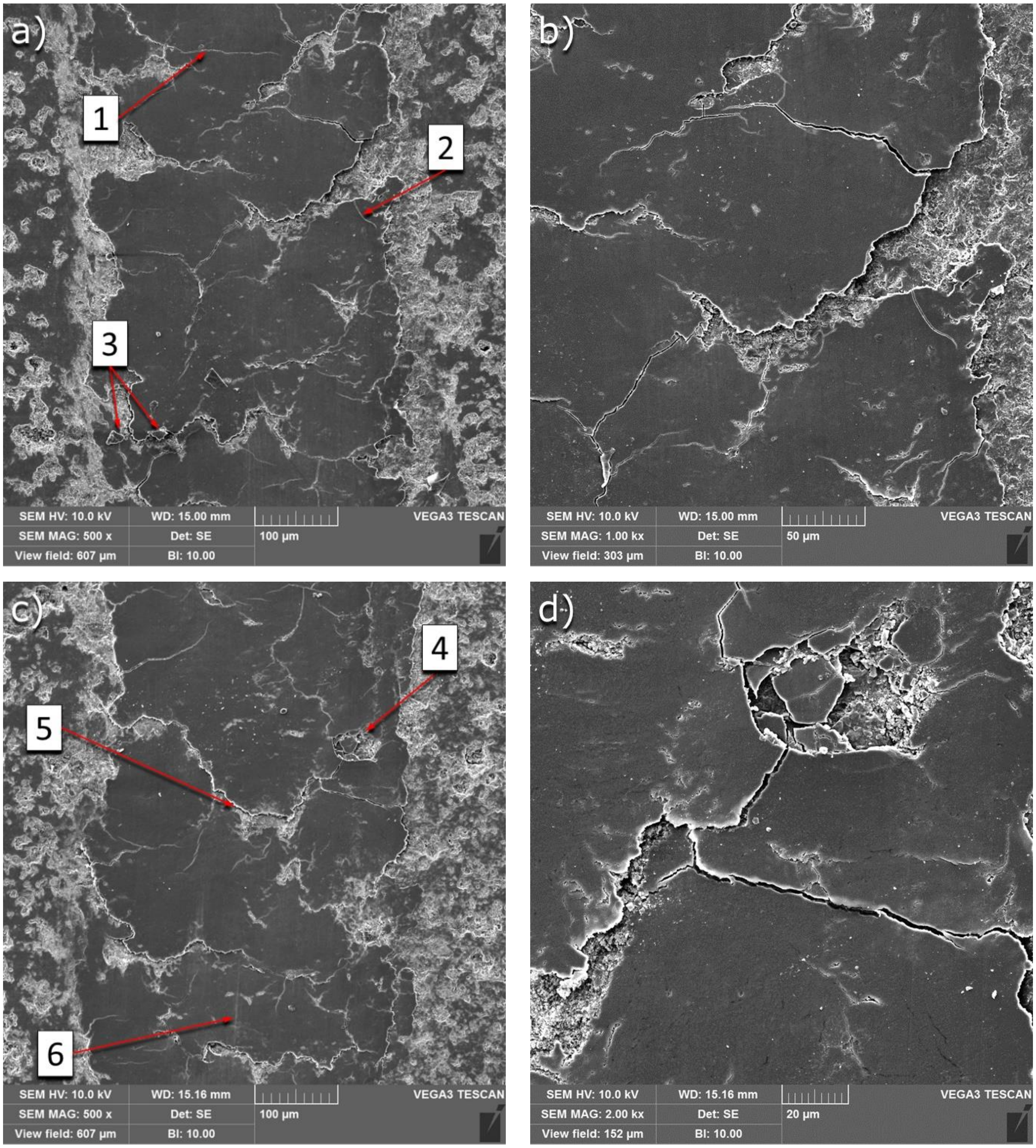

Fig. 6. The SEM observations of wear tracks of I80 sample: a) The examples of 1 – perpendicular cracks, 2 – scratches resulting from debris movement, 3 – debris; b) closer look at the example of splats delamination and scratches; c) the example of 4 – pore-induced cracking, 5 – delamination, 6 - sliding wear marks; d) closer look at the pore-induced cracking mechanism

CONCLUSIONS

In this paper, the impact of spraying distance and type of the injection system on morphology, mechanical properties, and wear resistance of Al_2O_3 + 13 wt.% TiO_2 coatings were examined and compared. The obtained results led to formulation of following conclusions:

The type of injection system significantly influenced coating characteristics. Internal injection led to a lower porosity level and higher hardness compared to external injection. Both properties are attributed to the extended exposure to heat, resulting in higher particle plasticity. Moreover, due to even heating regardless of particle size, the efficiency of the process was higher, resulting in a greater thickness of the coatings.

- Regardless of the type of the injection system, the higher spraying distance (100 mm) resulted in higher porosity, lower hardness, and higher wear rates. All these characteristics results from cooling down and resolidification of the in-flight particles.
- In all cases, the correlation between porosity, hardness and sliding wear resistance is visible. With the increase in porosity level, the decrease in hardness and sliding wear resistance is observed.
- The sample deposited using internal injection and spraying distance of 80 mm had the best outcome in case of hardness (966 HV0.2), porosity (4.1 %) and sliding wear resistance (18.55 $mm^3\ N^{-1}\ m^{-1} \cdot 10^{-6}$).
- The main mechanism of sliding wear was identified as low-cycle fatigue, as the surface of the wear tracks was marked with perpendicular cracks, typical for this mechanism. Additionally, the influence of the pores on wear mechanism was noticeable.

To conclude, the internal injection provides better heating condition, what results in formation of dense coatings of high sliding wear resistance. Moreover, this type of the injection system reduces the material loss during spraying resulting in better process efficiency. The proper adjustment of spraying distance may reduce the number of unmelted particles and allow formation of dense coating with compact structure.

Conflicts of Interest

The authors declare that they have no competing financial interests or personal relationships that could have seem to influence the study reported in this paper.

REFERENCES

1. Bolelli G, Cannillo V, Lusvarghi L, Manfredini T. Wear behaviour of thermally sprayed ceramic oxide coatings. Wear 2006;261. https://doi.org/10.1016/j.wear.2006.03.023.
2. Mayrhofer PH, Mitterer C, Hultman L, Clemens H. Microstructural design of hard coatings. Progress in Materials Science 2006;51. https://doi.org/10.1016/j.pmatsci.2006.02.002.
3. Bakan E, Vaßen R. Ceramic Top Coats of Plasma-Sprayed Thermal Barrier Coatings: Materials, Processes, and Properties. Journal of Thermal Spray Technology 2017;26. https://doi.org/10.1007/s11666-017-0597-7.
4. Heimann RB. Plasma-Spray Coating: Principles and Applications. 2007. https://doi.org/10.1002/9783527614851.
5. Boulos MI, Fauchais PL, Heberlein JVR. Thermal Spray Fundamentals: From Powder to Part, Second Edition. 2021. https://doi.org/10.1007/978-3-030-70672-2.

6. Pawlowski L. The Science and Engineering of Thermal Spray Coatings: Second Edition. 2008. https://doi.org/10.1002/9780470754085.
7. Nie X, Meletis EI, Jiang JC, Leyland A, Yerokhin AL, Matthews A. Abrasive wear/corrosion properties and TEM analysis of Al2O3 coatings fabricated using plasma electrolysis. Surface and Coatings Technology 2002;149. https://doi.org/10.1016/S0257-8972(01)01453-0.
8. Yilmaz R, Kurt AO, Demir A, Tatli Z. Effects of TiO_2 on the mechanical properties of the Al2O3-TiO2 plasma sprayed coating. Journal of the European Ceramic Society 2007;27. https://doi.org/10.1016/j.jeurceramsoc.2006.04.099.
9. Wang Y, Jiang S, Wang M, Wang S, Xiao TD, Strutt PR. Abrasive wear characteristics of plasma sprayed nanostructured alumina/titania coatings. Wear 2000;237:176–85. https://doi.org/10.1016/S0043-1648(99)00323-3.
10. Musalek R, Tesar T, Dudik J, Medricky J, Cech J, Lukac F. Cohesion of Dissimilar Splats in Hybrid Plasma-Sprayed Coatings: A Case Study for Al2O3-TiO2. Journal of Thermal Spray Technology 2022;31. https://doi.org/10.1007/s11666-022-01401-4.
11. Łatka L, Michalak M, Szala M, Walczak M, Sokołowski P, Ambroziak A. Influence of 13 wt% TiO2 content in alumina-titania powders on microstructure, sliding wear and cavitation erosion resistance of APS sprayed coatings. Surface and Coatings Technology 2021;410:126979. https://doi.org/10.1016/J.SURFCOAT.2021.126979.
12. Goberman D, Sohn YH, Shaw L, Jordan E, Gell M. Microstructure development of Al2O3–13wt.%TiO2 plasma sprayed coatings derived from nanocrystalline powders. Acta Materialia 2002;50:1141–52. https://doi.org/10.1016/S1359-6454(01)00414-1.
13. Palanivelu R, Kumar AR. Scratch and wear behaviour of plasma sprayed nano ceramics bilayer Al_2O_3-13 wt%TiO_2/hydroxyapatite coated on medical grade titanium substrates in SBF environment. Appl Surf Sci 2014;315:372–9. https://doi.org/10.1016/J.APSUSC.2014.07.167.
14. Nowakowska M, Łatka L, Sokołowski P, Szala M, Toma FL, Walczak M. Investigation into microstructure and mechanical properties effects on sliding wear and cavitation erosion of Al_2O_3–TiO_2 coatings sprayed by APS, SPS and S-HVOF. Wear 2022;508–509. https://doi.org/10.1016/j.wear.2022.204462.
15. Vardelle M, Vardelle A, Fauchais P. Spray parameters and particle behavior relationships during plasma spraying. Journal of Thermal Spray Technology 1993;2. https://doi.org/10.1007/BF02647426.
16. Jafarzadeh K, Valefi Z, Ghavidel B. The effect of plasma spray parameters on the cavitation erosion of Al2O3–TiO2 coatings. Surface and Coatings Technology 2010;205:1850–5. https://doi.org/10.1016/J.SURFCOAT.2010.08.044.
17. Abbas RA, Ajeel SA, Ali Bash MA, Kadhim MJ. Effect of plasma spray distance on the features and hardness reliability of YSZ thermal barrier coating. Materials Today Proceedings 2021;42. https://doi.org/10.1016/j.matpr.2020.12.578.
18. Song EP, Ahn J, Lee S, Kim NJ. Effects of critical plasma spray parameter and spray distance on wear resistance of Al2O3-8 wt.%TiO2 coatings plasma-sprayed with nanopowders. Surface and Coatings Technology 2008;202. https://doi.org/10.1016/j.surfcoat.2008.01.002.
19. Vardelle M, Fauchais P, Vardelle A, Li KI, Dussoubs B, Themelis NJ. Controlling particle injection in plasma spraying. Journal of Thermal Spray Technology 2001;10:267–84. https://doi.org/10.1361/105996301770349367.

20. Liu SH, Trelles JP, Li CJ, Li CX, Guo HB. A review and progress of multiphase flows in atmospheric and low pressure plasma spray advanced coating. Materials Today Physics 2022;27:100832. https://doi.org/10.1016/J.MTPHYS.2022.100832.

21. Martínez-Villegas I, Mora-García AG, Ruiz-Luna H, Mckelliget J, Poblano-Salas CA, Muñoz-Saldaña J, et al. Swirling Effects in Atmospheric Plasma Spraying Process: Experiments and Simulation. Coatings 2020;10:388. https://doi.org/10.3390/coatings10040388.

22. Łatka L, Michalak M, Jonda E. Atmospheric Plasma Spraying of Al_2O_3 + 13% TiO_2 Coatings Using External and Internal Injection System. Advances in Materials Science 2019;19. https://doi.org/10.2478/adms-2019-0018.

23. ASTM International. ASTM G99-19: Standard Test Method for Wear Testing with a Pin-on-Disk Apparatus. Book of Standards 2017. https://doi.org/10.1520/G0099-17.

24. Michalak M, Łatka L, Sokołowski P, Niemiec A, Ambroziak A. The Microstructure and Selected Mechanical Properties of Al_2O_3+13 wt % TiO_2 Plasma Sprayed Coatings. Coatings 2020;10. https://doi.org/10.3390/coatings10020173.

25. ASTM International. ASTM E2109-01: Standard Test Methods for Determining Area Percentage Porosity in Thermal Sprayed Coatings. Book of Standards 2021. https://doi.org/10.1520/E2109-01R21.

26. EN ISO 4516: Metallic and other Inorganic Coatings—Vickers and Knoop Microhardness Tests; Swiss Association for Standardization. Winterthur, Switzerland: 2004.

27. Lancaster JK. The influence of substrate hardness on the formation and endurance of molybdenum disulphide films. Wear 1967;10:103–17. https://doi.org/10.1016/0043-1648(67)90082-8.

28. Xue M, Lai X, Wang J, Liu S, Wang X, Jiang K. Microstructure and high-temperature sintering properties of APS coatings prepared from spherical thin-walled hollow-shell powders. Ceramics International 2022;48:31652–60. https://doi.org/10.1016/J.CERAMINT.2022.07.086.

29. Kulkarni A, Vaidya A, Goland A, Sampath S, Herman H. Processing effects on porosity-property correlations in plasma sprayed yttria-stabilized zirconia coatings. Materials Science and Engineering: A 2003;359:100–11. https://doi.org/10.1016/S0921-5093(03)00342-3.

30. Mutter M, Mauer G, Mücke R, Guillon O, Vaßen R. Correlation of splat morphologies with porosity and residual stress in plasma-sprayed YSZ coatings. Surface and Coatings Technology 2017;318:157–69. https://doi.org/10.1016/J.SURFCOAT.2016.12.061.

31. Sampath S, Jiang XY, Matejicek J, Leger AC, Vardelle A. Substrate temperature effects on splat formation, microstructure development and properties of plasma sprayed coatings Part I: Case study for partially stabilized zirconia. Materials Science and Engineering: A 1999;272:181–8. https://doi.org/10.1016/S0921-5093(99)00459-1.

32. Mauer G, Vaßen R, Stöver D, Kirner S, Marqués J-L, Zimmermann S, et al. Improving Powder Injection in Plasma Spraying by Optical Diagnostics of the Plasma and Particle Characterization. Journal of Thermal Spray Technology 2011;20:3–11. https://doi.org/10.1007/s11666-010-9577-x.

33. Odhiambo JG, Li W, Zhao Y, Li C. Porosity and Its Significance in Plasma-Sprayed Coatings. Coatings 2019;9:460. https://doi.org/10.3390/coatings9070460.

34. Zhou J, Sun K, Huang S, Cai W, Wei Y, Meng L, et al. Fabrication and Property Evaluation of the Al2O3-TiO2 Composite Coatings Prepared by Plasma Spray. Coatings 2020;10:1122. https://doi.org/10.3390/coatings10111122.

35. Kwon H, Yoo YW, Park Y, Nam UH, Byon E. Effect of TiO2 on mechanical and thermal properties of Al2O3-based coating via atmospheric plasma spraying. Journal of Asian Ceramic Societies 2023;11. https://doi.org/10.1080/21870764.2023.2203991.

36. Shen Y, Tao H, Lin Y, Zeng X, Wang T, Tao J, et al. Fabrication and Wear Resistance of TiO2/Al2O3 Coatings by Micro-arc Oxidation. Rare Metal Materials and Engineering 2017;46:23–7. https://doi.org/10.1016/S1875-5372(17)30071-1.

37. Jeong DH, Erb U, Aust KT, Palumbo G. The relationship between hardness and abrasive wear resistance of electrodeposited nanocrystalline Ni–P coatings. Scripta Materialia 2003;48:1067–72. https://doi.org/10.1016/S1359-6462(02)00633-4.

38. Wang Y, Jiang S, Wang M, Wang S, Xiao TD, Strutt PR. Abrasive wear characteristics of plasma sprayed nanostructured alumina/titania coatings. Wear 2000;237:176–85. https://doi.org/10.1016/S0043-1648(99)00323-3.

39. Fletcher DI, Corteen J, Wilby A. Rough surface rolling contact fatigue crack stress intensity factor calculation for modern rail steels. Wear 2024;540–541:205231. https://doi.org/10.1016/J.WEAR.2023.205231.

40. Rabinowicz E, Dunn LA, Russell PG. A study of abrasive wear under three-body conditions. Wear 1961;4. https://doi.org/10.1016/0043-1648(61)90002-3.

41. Klyatskina E, Espinosa-Fernández L, Darut G, Segovia F, Salvador M D, Montavon G, et al. Sliding Wear Behavior of Al 2 O 3-TiO2 Coatings Fabricated by the Suspension Plasma Spraying Technique. Tribology Letters 2015;59. https://doi.org/10.1007/s11249-015-0530-5.